

## Angle dependence of magnetization in a single-domain $\text{YBa}_2\text{Cu}_3\text{O}_x$ sphere

B. A. Tent, D. Qu, and Donglu Shi

*Department of Materials Science and Engineering, University of Cincinnati, Cincinnati, Ohio 45211*

W. J. Bresser and P. Boolchand

*Department of Electrical and Computer Engineering and Computer Science, University of Cincinnati, Cincinnati, Ohio 45211*

Zhi-Xiong Cai

*Materials Science Division, Brookhaven National Laboratory, Upton, New York 11973*

(Received 18 March 1998; revised manuscript received 16 June 1998)

The crystal angle dependence of magnetization has been measured in spherically shaped, single-domain  $\text{YBa}_2\text{Cu}_3\text{O}_x$  (YBCO). The single-domain sample is processed by a seeded-melt growth process in which a small  $\text{NdBa}_2\text{Cu}_3\text{O}_x$  seed is used to induce domain growth through a peritectic reaction in YBCO. It has been found that the angle dependence of magnetization can be obtained in a series of zero-field-cooled hysteresis loop measurements with warm-ups well above  $T_c$  between each measurement at a specific angle. In contrast to previously reported results, we have found that the angle dependence exhibits a sawtooth wave between  $0^\circ$  and  $360^\circ$  over a wide range of temperatures and fields. Furthermore, we have also measured the angle dependence on a YBCO plate and found similar behavior, indicating that the sawtooth wave is intrinsic to the superconductor. A physical model has been developed to explain the angle dependence of magnetization observed in this experiment. [S0163-1829(98)05541-6]

### INTRODUCTION

In our previous work,<sup>1,2</sup> we have measured the angle dependence of levitation force in a  $\text{YBa}_2\text{Cu}_3\text{O}_x$  (YBCO) sphere which was processed by a so-called seeded-melt growth method.<sup>3-5</sup> The sphere, 6.2 mm in diameter, has a single-crystal characteristic with only one domain in the sample. The angle dependence of the levitation force exhibits a cosine law between  $0^\circ$  and  $360^\circ$  at 77 K. We have used a magnetic dipole model to explain the angle dependence.<sup>1,2</sup> Such a pronounced angle dependence originates from the superconducting anisotropy of high-temperature superconductors (HTS's), which was extensively studied by neutron diffraction,<sup>6</sup> transport resistivity measurements,<sup>7</sup> and critical current density studies.<sup>8</sup> The previous experimental results indicate that the high electron conduction along the  $ab$  plane in the unit cell of YBCO is responsible for the pronounced anisotropy in many superconducting parameters including critical current density  $J_c$ , magnetization  $M$ , susceptibility  $\chi$ , resistivity  $\rho$ , and upper critical fields  $H_{c2}$ . Furthermore, as a result of the two-dimensional electron conduction nature of YBCO, it has been observed that the resistivity transition is severely broadened in a magnetic field,<sup>9</sup> which in turn yields extremely high upper critical fields compared to those of low- $T_c$  superconductors.<sup>10</sup> Of particular importance are the superconducting anisotropy and its effect on the vortex state especially for the Bi-Sr-Ca-Cu-O (BSCCO) compounds. Due to BSCCO's higher degree of structural anisotropy, vortices are decoupled at moderate temperatures and fields.<sup>11,12</sup> After decoupling, the vortices behave like two-dimensional pancakes that are difficult to pin down by crystal defects. As a consequence, the critical current density decreases drastically in the presence of a magnetic field, which has been the major

obstacle for industrial applications of high-temperature superconductors.

In an investigation of the angle dependence of magnetization, Gyorgy *et al.* measured magnetization of a YBCO single crystal and determined the anisotropic critical currents by using an extended Bean model.<sup>8</sup> The single-crystal samples that they used had an average dimension of  $2 \times 2 \times 0.1$  mm<sup>3</sup>. They further noted that the crystals were plate-like with the smallest dimension along the  $c$  axis, which were typical samples commonly used for both transport and magnetic measurements in previous studies. In their measurements, by using a vibrating sample magnetometer (VSM), the sample was cooled to a given temperature in zero field first. The field was then applied to induce magnetization. After the establishment of the field, the sample was rotated to change the angle from  $0^\circ$  to  $90^\circ$ . They found that the magnetic hysteresis difference  $\Delta M$  increased from below 50 G to about 700 G in a sine law fashion as the angle (defined as the angle between the applied field and  $ab$  plane) was changed from  $0^\circ$  to  $90^\circ$ . Using the extended Bean model that they proposed, they were able to explicitly account for the presence of anisotropic critical currents that are proportional to  $\Delta M$ .

As is well known, magnetic measurements suffer from demagnetization that is attributed to the geometry of the sample.<sup>13</sup> In particular, as a platelike sample is rotated in the measurement, the geometric variation along the axis of the applied field becomes even more complicated, which cannot be easily ruled out by accounting for the demagnetization factor. Therefore, the correction for magnetization has been a serious problem in the study of angle dependence and, hence, the anisotropy.

In this paper, we report magnetization values of a spherically shaped, single-domain  $\text{YBa}_2\text{Cu}_3\text{O}_x$ , at various crystal

orientations. Such a sphere will ensure that no geometric effects will be encountered by rotation of the sample about the central axis. The spherical sample has a single-crystal characteristic in terms of crystallographic and electromagnetic properties. The sample was obtained by using a specially designed grinding apparatus, after the samples were sectioned from a large single-domain material processed by the so-called seeded-melt growth (SMG) method. We propose a model to explain the observed behavior and discuss the possible physical mechanisms.

### SAMPLE PREPARATION

The samples used in this experiment were sectioned from a large single-domain material processed by the SMG method. Melt growth processing has been previously reported.<sup>14–20</sup> The SMG method<sup>1–5</sup> utilized here involved a modified peritectic solidification from a partial melt above 1010 °C. Here 25 g of precursor material was thoroughly mixed and pressed into a hexagonal shape with a face diagonal length of 29 mm. A thin  $\text{NdBa}_2\text{Cu}_3\text{O}_x$  single crystal of dimension  $1.5 \times 1.5 \times 0.5 \text{ mm}^3$  was placed at the center of the top surface of the green pellet. A vertical tube furnace with a small vertical temperature gradient of 3–5 °C/cm was used for SMG processing. The sample was placed in the furnace and heated with a 100 °C/h ramp rate until the final temperature of 1055 °C was reached. The sample was held at this temperature for 3 h in order to achieve a homogeneous melt. The furnace was then cooled at 10 °C/h to 1020 °C and further cooled to 980 °C/h at 1 °C/h, at which point the domain growth of the sample was completed. The furnace was then cooled at the much faster rate of 100 °C/h to room temperature. The final materials possessed a single-domain structure.<sup>1–5</sup> The SMG-processed samples were then oxygenated in flowing  $\text{O}_2$  at 400 °C for 7 days.

The next step involved sectioning and shaping the SMG-processed sample in order to obtain the desired shape. The single-domain sample was initially sectioned and the interior portion of each section was examined for domain orientation using optical and scanning electron microscopy. The samples were then hand ground to a roughly spherical shape and attained their final spherical shape only after being placed in an aluminum hemisphere lined with SiC powder and mechanically ground by the action of a compressed air jet. The final diameter of the sample is 6.2 mm (see Fig. 1). Each sphere was then oxygenated again in flowing  $\text{O}_2$  at 400 °C for 4 days to ensure homogeneity. After oxygenation, each sample was then inspected individually, utilizing a variety of microscopy techniques so as to determine the precise domain orientation. With the crystal orientation definitely determined, each sample was mounted on the end of a modified magnetometer sample holder such that the  $c$  axis of the sample was perpendicular to the long axis of the holder.

### MAGNETIZATION MEASUREMENTS

The magnetic measurements obtained in this study were conducted with an E, G & G model 4500 VSM. This instrument is computer controlled and able to facilitate a wide range of magnetic moments measurements. The instruments magnetic sensitivity ranges from  $5 \times 10^{-5}$  to  $1 \times 10^4$  emu.

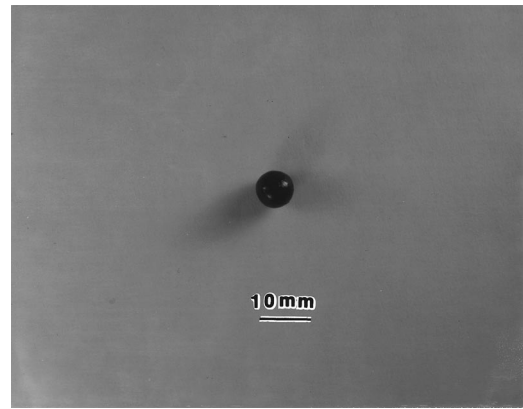


FIG. 1. Optical photograph showing a spherical  $\text{YBa}_2\text{Cu}_3\text{O}_x$  sample.

The VSM, equipped with a helium vapor refrigeration unit, is also capable of measurements ranging from room temperature down to 5 K. The temperature in the sample chamber is monitored electronically and is held constant for emu vs oerstead measurements. The applied magnetic field of the VSM is monitored by a built-in Hall-effect gaussmeter that provides a feedback signal to the primary controller. This feedback signal allows the power supplied to the magnet to be monitored and, consequently, the intensity of the applied magnetic field to be adjusted, which provides the capability for both static and field sweep measurements.

The YBCO sphere sample is mounted on the end of a threaded sample holder that is, in turn, screwed on to a long sample rod assembly as shown in Fig. 2. The sample rod assembly consists of a long brass rod with an additional quartz rod firmly affixed to the end. The length of the rod is fixed so that the attached sample is seated precisely between two pickup coils attached to each pole piece of the laboratory

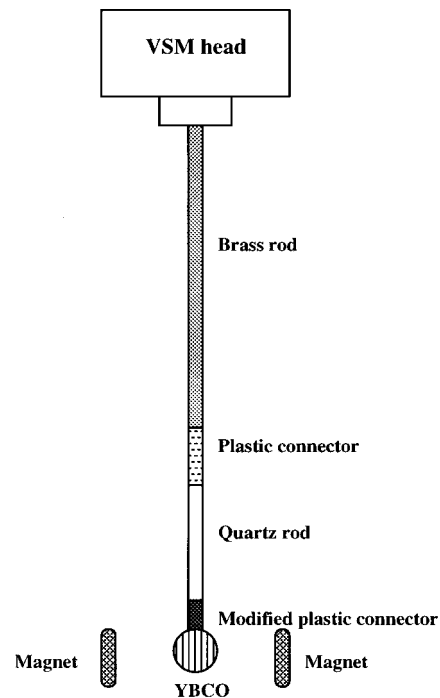


FIG. 2. Schematic diagram showing the sample mounting assembly.

magnet. The sample holder to which the HTS sample is connected is designed to hold small volumes of liquid, powder, or bulk samples. Due to the volume of the sample used in this experiment, the sample holder was modified to accommodate a 6.2-mm sphere. The small chamber that was to hold a standard sample was machined down to a flat surface, and small holes were drilled along the long axis of the holder. The YBCO sample was then affixed to the flattened end of the holder with conductive varnish. Nylon thread was run through the drilled holes in order to form a basketlike structure around the sample. This was to prevent the sample from falling to the bottom of the sample chamber should it become detached. Once the sample had been firmly affixed to the sample rod, the entire assembly was lowered into the sample chamber. The end of the assembly opposite the sample is then threaded into the head of the VSM.

In our VSM measurement, we used two different procedures to obtain the angle dependence of magnetization. The first procedure is similar to the previously reported method<sup>8</sup> and was conducted to determine the angle dependence of the induced magnetic moment. The initial measurement was carried out at 70 K with the  $c$  axis of the sample initially oriented parallel to the applied field. The magnetic field was set at a constant value and the magnet turned on. The magnetic moment of the sample at this orientation was then recorded and the sample rotated  $10^\circ$  by turning the magnetometer head. This procedure was repeated every  $10^\circ$ , up to  $360^\circ$ , while maintaining a constant magnetic field. The measurement was then repeated for a variety of other field strength values, both high and low. In this manner, a profile of the magnetic moment versus sample orientation was developed for one full revolution of the sample.

The second procedure involved warm-ups between measurements at a particular orientation. Initially, the sample was placed in the magnetometer such that the  $c$  axis of the sample was parallel to the direction of the field between the two pole pieces. A series of magnetic hysteresis loops was then collected with the sample in this position for a range of temperatures from 80 to 15 K (the stability limit of the instrument). Between each measurement, the sample was warmed to above the superconducting transition temperature in order to expel any trapped flux and therefore maintain a zero-field cool (ZFC) for each subsequent measurement. A second series of measurements was conducted with the sample oriented perpendicular to the applied magnetic field. Through these two sets of measurements, a profile of the magnitude of the induced magnetic moment with respect to temperature was obtained for the two primary orientations of the sample.

Another set of measurements was then ascertained in a similar fashion. The YBCO sample was placed in the magnetic field such that the  $c$  axis of the material was parallel to the applied field. A hysteresis measurement was then collected for this orientation at a given temperature (for instance, at 70 K). The sample was then warmed up to above the transition temperature to provide a trapped flux relief. After advancing the sample by  $10^\circ$ , the system was cooled back down to 70 K and another hysteresis measurement was taken. This measurement was repeated for orientations between  $0^\circ$  and  $90^\circ$ . These measurements provided another, more accurate means of attaining an orientation dependence

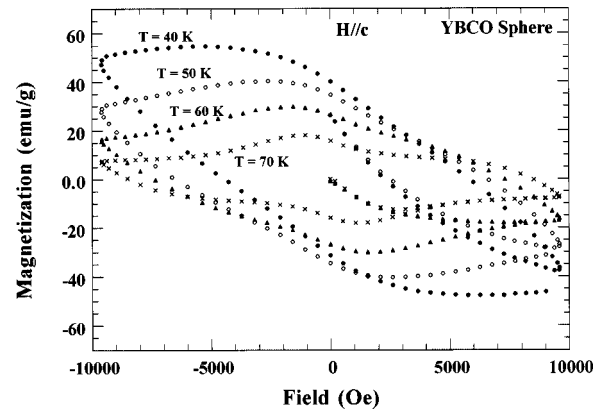


FIG. 3. Magnetic hysteresis loops with  $\mathbf{H}\parallel c$  at the temperatures indicated.

of the induced magnet moment of the material. In order to illustrate the critical nature of sample shape on these measurements, an identical set of all three measurements was made on a thin plate of HTS material. The results of these measurements will be discussed later.

## RESULTS AND DISCUSSION

Figure 3 shows the magnetization hysteresis curves for the YBCO sphere oriented with the  $c$  axis parallel to the field obtained at 40, 50, 60, and 70 K by using the first procedure (i.e., no warm-ups between measurements). As can be seen in this figure, due to strong pinning and large volume of the sample, the applied field begins to significantly penetrate the superconductor at rather high temperatures near 60 K. It was found that the field penetration became difficult below 20 K, and the full penetration field  $H^*$  is assumed to be much higher than the applied field of 1 T that is available in this experiment. Figure 4 shows the pronounced anisotropy observed in the YBCO sphere. The magnetic hysteresis along the  $c$  axis has been found to be 5 times greater than that along the  $ab$  plane at 3000 G, which is consistent with the previous studies.

Using the first experimental procedure, we have obtained the angle dependence data for magnetization of the YBCO sphere. The data points are shown in Fig. 5. As can be seen

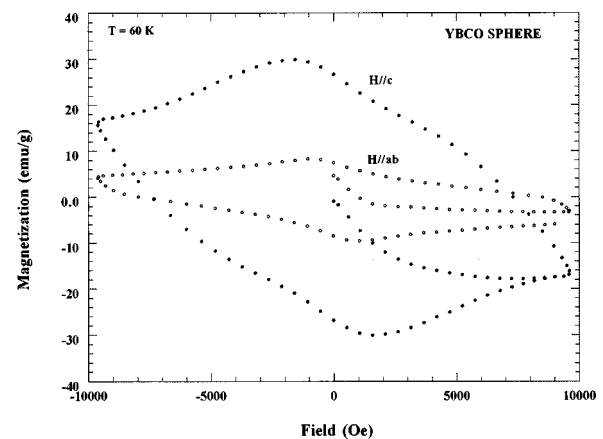


FIG. 4. Magnetic hysteresis loops with  $\mathbf{H}\parallel c$  and  $\mathbf{H}\parallel ab$  at the temperature indicated. The anisotropy at 2000 G is about 5.

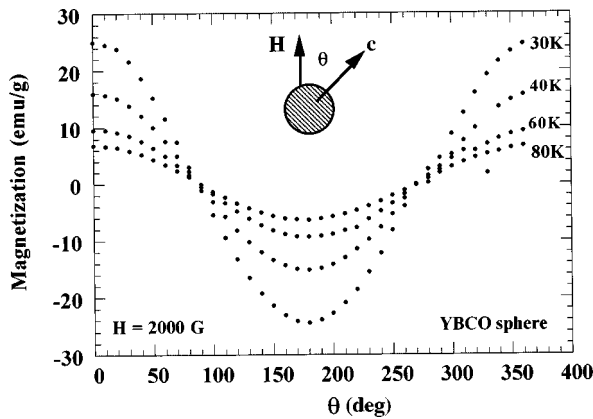


FIG. 5. Magnetization vs angle at 2000 G and the temperatures indicated. No flux line relief is employed above  $T_c$  between each rotation of the sample.

in Fig. 5, the angle dependence of magnetization in a wide temperature range (30–80 K) exhibits a cosine law behavior. It should be noted that the initial positive magnetization was a result of the trapped flux from previous magnetic hysteresis measurements. However, in this particular measurement, we are only interested in the angle dependence behavior, but not the specific values of magnetization. Figure 6 shows the angle dependence of magnetization measured in the same way, but at much lower fields ( $H = 1 - 15$  G) at two different temperatures  $T = 20$  and 70 K. As can be seen, the same behavior is observed compared to that shown in Fig. 5.

The behavior illustrated by Figs. 4 and 5 is similar to that reported by Gyorgy *et al.* on single-crystal YBCO samples.<sup>8</sup> This is important to note as it indicates that the presence of low-angle grain boundaries within a sample is not critical to the measure of angle dependence. Furthermore, previous work by Shi and co-workers<sup>1-5</sup> has demonstrated that the low-angle grain boundaries are within the range of a few degrees and would hardly serve as a detriment to the effect of angle dependence.

The  $\cos \theta$  dependence of the magnetization is in agreement with the levitation force measurement that we reported previously. In the study of the angle dependence of the levitation force, we assumed the superconductor to be a magnetic dipole which interacts with the permanent test magnet.

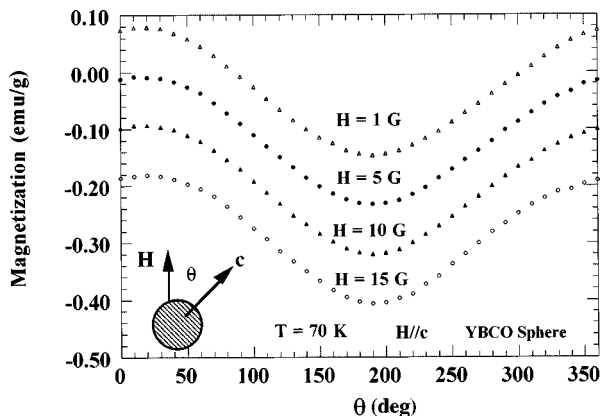


FIG. 6. Magnetization vs angle at 70 K and fields indicated. No flux line relief is employed above  $T_c$  between each rotation of the sample.

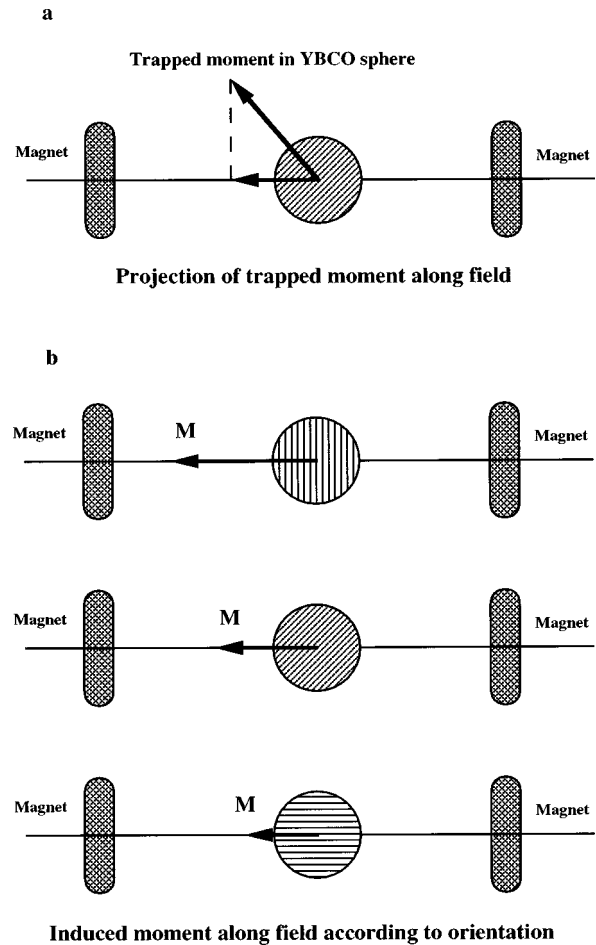


FIG. 7. Schematic diagrams showing (a) a strongly trapped moment in the YBCO sphere (the rotation of the sample results in merely a projection of the moment along the applied field) and (b) an induced moment along the direction of the field according to the orientation. Note that, in the second procedure, the induced moment is always parallel to the applied field.

Using this dipole model, we have successfully described the cosine angle dependence of the levitation force in the YBCO sphere.<sup>2</sup> In this study, we use the same approach by assuming that the YBCO sphere is a magnetic dipole in the presence of an applied field as schematically illustrated in Fig. 7. As illustrated, below  $T_c$ , the superconductor will respond to the externally applied field by establishing an internal induction  $B$ . This induced moment is highest when the  $c$  axis is parallel to the applied field, and as a result of anisotropy, it decreases as the  $c$  axis rotates away from the direction of the field. The measured magnetic moment will be the projection of the dipole moment along the direction of the field as can be seen in Fig. 7. As the dipole is rotated to the position normal to the applied field ( $\theta = 90^\circ$ ), the projection will then be zero, which is seen from Figs. 5 and 6. Further rotation will result in another maximum at  $180^\circ$  and a minimum at  $270^\circ$  as can also be seen in Figs. 5 and 6.

An important point to be noted here is that the angle dependence, as observed in Figs. 5 and 6, does not reflect superconducting anisotropy, but rather the projection of a trapped magnetic field. It is also to be noted that most of the previous work had employed the same method similar to our “first procedure” for the “angle dependence” study. In fact,

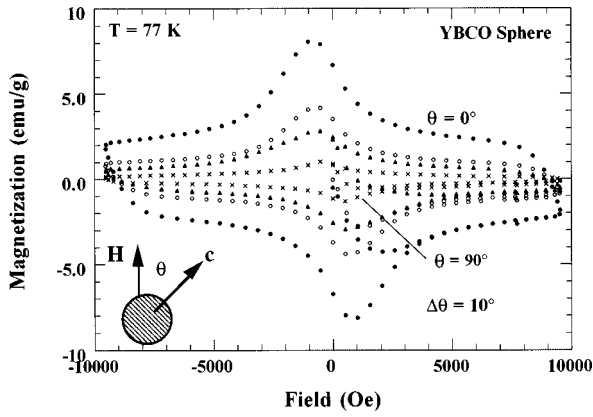


FIG. 8. Magnetic hysteresis loops taken between 0° and 90° with a 10° interval at 77 K. Flux line relief is employed above  $T_c$  between each rotation of the sample.

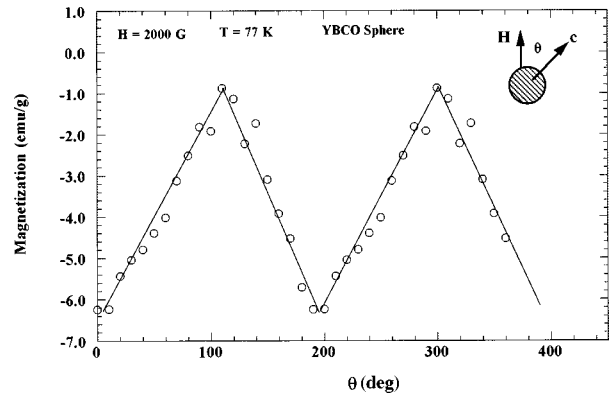


FIG. 9. Magnetization vs angle of the YBCO sphere at 77 K and 2000 G. The data points are taken from the hysteresis loops shown in Fig. 8.

any superconductors including those isotropic low- $T_c$  materials will exhibit the behavior shown in Figs. 5 and 6 as long as the sample can trap significant magnetic field due to strong pinning. Therefore, a true angle dependence reflecting superconducting anisotropy must be obtained through a different approach as we described in the “second procedure.” In this procedure, the sample is cooled in zero field below  $T_c$  first. A field is then applied to induce a dipole moment in the superconductor. This induced field is closely associated with the orientation of the  $ab$  planes with respect to the applied field. After recording a magnetic moment value at a specific orientation, the sample must be warmed up to above  $T_c$  to remove all the trapped flux lines. The sample is rotated to assume another orientation and cooled in zero field to below  $T_c$ . After the application of the field, a different moment will be induced in the superconductor that is directly related to the new orientation of the superconductor. A major difference between the first and second procedures is that the former results in a trapped moment rotating with respect to the direction of the field and the registered magnetic moment is merely its projection. The latter ensures that the induced moment is always pointing in the direction of the applied field with a varied magnitude that is determined by the superconducting anisotropy. Therefore, only in the second procedure can one truly measure the angle dependence and hence the anisotropy of the superconductor.

Following the second procedure, we have measured the true angle dependence of the YBCO sphere. As shown in Fig. 8, the magnetic hysteresis loops of the YBCO sphere were obtained at 70 K and at some representative (0°, 40°, 60°, and 90°) angles indicated. The sample was warmed up to 150 K, well above  $T_c$ , between each hysteresis measurement ensuring a ZFC condition for each specific angle. Based on these hysteresis loops, the magnetization values at some applied fields were chosen and plotted against orientation angles as shown in Fig. 9. As shown in Fig. 9, the angle dependence of magnetization at  $H = 2000$  G, exhibits a sawtooth wave between 0° and 360°, which is distinctively different from the cosine law behavior shown in Figs. 5 and 6. For comparison, we have also, in the exact same way, measured the angle dependence of a YBCO plate of dimension  $4 \times 4 \times 1$  mm<sup>3</sup>, which is processed by the seeded-melt growth method (e.g., the sample has a single-domain struc-

ture). Figure 10 shows the magnetization versus angle for the YBCO plate. As shown in Fig. 10, a similar sawtooth behavior is again observed in the YBCO plate sample. From the data shown in Figs. 9 and 10, we can see that the sawtooth behavior is not influenced by the geometry of the sample and is therefore intrinsic to the single-domain YBCO.

A mathematical expression for the sawtoothlike behavior shown in Figs. 9 and 10 was developed using London equations and Bean model of flux penetration (both were discussed earlier). We assume that the magnetization of the sample stems directly from a circulating supercurrent induced within the superconducting material by the external magnetic field. Consider a sphere as sketched in Fig. 11(b). Such a sphere has an anisotropic critical current density in the  $ab$  plane ( $J_c^{ab}$ ) and  $c$  direction such that  $J_c^{ab} \gg J_c^c$ . As we will show, the relative magnitude of these two quantities is key to determine the features in Figs. 9 and 10.

We start with the London equation

$$\nabla \times \mathbf{B} = \mu_0 \mathbf{J}_s, \tag{1}$$

where the effective field  $\mathbf{B} = \mu_0 \mathbf{H} + \mathbf{M}$ , and  $\mathbf{H}$  and  $\mathbf{M}$  are the applied external magnetic field and the local magnetization, respectively.  $\mathbf{J}_s$  is the local supercurrent density. At the surface of the sphere, the local magnetization of the sample,  $\mathbf{M}$ ,

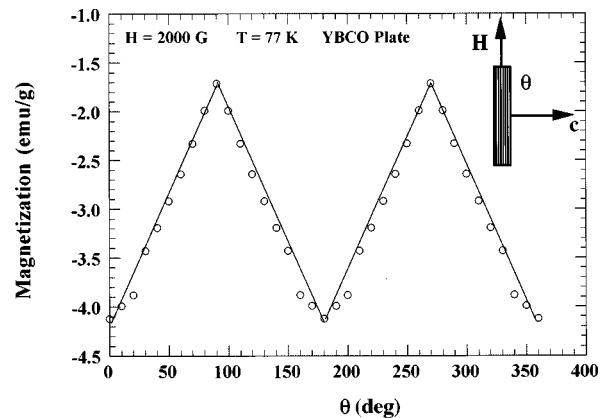


FIG. 10. Magnetization vs angle of a YBCO plate at 77 K and 2000 G.

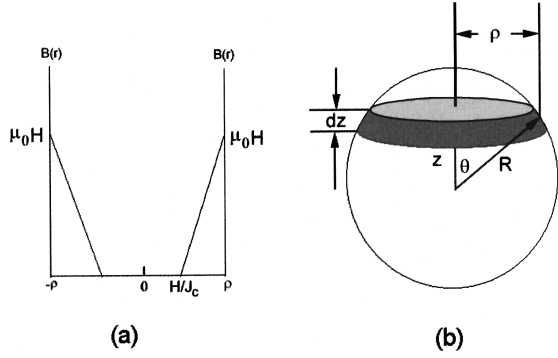


FIG. 11. (a) Profile of the magnetic inductance of a superconducting sample according to the Bean model.  $\mathbf{B} = \mu_0 \mathbf{H}$  at the surface of the sample and decreases linearly with the depth into the sample with slope equal to the critical current density  $J_c$ . (b) Schematic diagram of a superconducting sphere with radius  $R$  in which a circular disk is shown with thickness  $dz$  and radius  $\rho = R \sin \theta$ , where  $R$  is the radius of the sphere.

goes to zero and therefore  $\mathbf{B} = \mu_0 \mathbf{H}$ . Substituting this into the London equation above and rewriting Eq. (1) in integral form yields

$$B(r) = \mu_0 H + M(r). \quad (2)$$

We can then see that the local magnetization  $\mathbf{M}(\mathbf{r})$  is such that

$$M(r) = \mu_0 \int_r^\rho J_s d\mathbf{r}'. \quad (3)$$

Using the Bean model as illustrated in Fig. 11(a), we assume that  $J_s$  equals the critical current density  $J_c$  near the surface of the sample and  $J_c$  is constant throughout the sample. This leads to

$$M(r) = \mu_0 J_c (\rho - r) \quad (4a)$$

for  $H/J_c < r < \rho$  and

$$M(r) = \mu_0 H \quad (4b)$$

for  $0 < r < H/J_c$ . Equations (4a) and (4b) assume  $\rho > H/J_c$ . For  $\rho > H/J_c$ , the magnitude of the local magnetization is expressed as

$$M(r) = \mu_0 J_c (\rho - r). \quad (5)$$

It is important to note that up to this point we have made no assumption with regards to the size of the sample.

Now consider a ‘‘slice’’ of the sphere that is a circular disk with radius  $\rho = R \sin \theta$  and has a thickness  $dz$  as shown in Fig. 11(b). The total magnetic moment of such a disk can be written as

$$m(\rho, z) = m(\rho) dz = \int_0^\rho M(r) 2\pi r dr dz. \quad (6)$$

Substituting Eqs. (4) and (5) into Eq. (6) results in

$$m(\rho) = \pi \mu_0 H (\rho^2 - H\rho/J_c + H^2/J_c^2) \quad \text{for } \rho > H/J_c, \\ m(\rho) = \mu_0 J_c \rho^3/3 \quad \text{for } \rho < H/J_c. \quad (7)$$

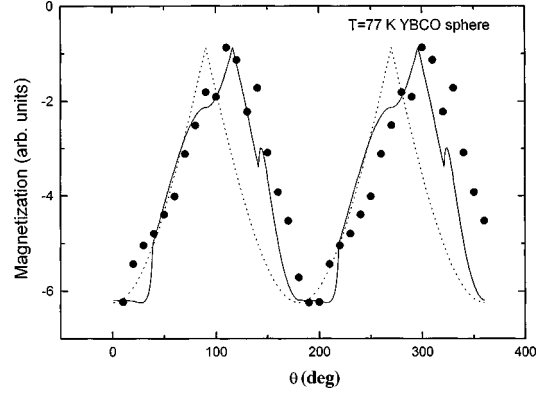


FIG. 12. Orientation dependence of magnetization of a YBCO sphere with  $R = 6.2$  mm,  $J_c^{ab} = 8 \times 10^3$  A/cm<sup>2</sup>,  $J_c^{ab}/J_c^c = 5$ , and  $H = 2000$  G. The solid line is calculated from Eqs. (10)–(13). The dotted line is the ‘‘dipole’’ limit. The solid circles are the experimental data. The calculated results are scaled to the experimental data.

Substituting Eq. (7) into Eq. (6) and noting that  $\rho = R \sin \theta$ , we can then calculate the total magnetic moment of the entire sphere by integration over each slice such that

$$m = 2 \int_0^R m(\rho) dz = 2 \int_0^{\pi/2} m(R \sin \theta)^2 d\theta. \quad (8)$$

The average magnetization of the sphere is then

$$M = \frac{m}{4\pi R^3/3}. \quad (9)$$

For  $R < H/J_c$ , the magnetization of the sphere  $M$  can be written as

$$M = \frac{3}{32} \pi \mu_0 J_c R. \quad (10)$$

For  $R > H/J_c$ , the magnetization  $M$  can be written as

$$M(H, J_c) = \frac{3}{4} \mu_0 H \left\{ \frac{\sin^{-1}(H/J_c R)}{4(H/J_c R)} - \left( \frac{H}{J_c R} \right) \cos^{-1} \left( \frac{H}{J_c R} \right) \right. \\ \left. + \left[ \frac{13}{12} + \frac{3}{2} \left( \frac{H}{J_c R} \right)^2 \right] \sqrt{1 - \left( \frac{H}{J_c R} \right)^2} \right\}. \quad (11)$$

For Eqs. (10) and (11) we can see that  $H/J_c R$  is an important parameter for the magnetization of the superconducting sphere. If  $H/J_c R < 1$ , the magnetization displays an extreme sensitivity to the external field  $H$ . For  $H/J_c R \ll 1$ , we can disregard higher-power terms of  $H/J_c R$  in Eq. (11). That results in

$$M \approx \mu_0 H, \quad (12)$$

which is the result for the low-field, high-critical-current-density case.

The magnetization  $M$  of a YBCO sphere of any orientation with respect to  $H$  can be calculated from its components along the  $ab$  plane and  $c$  axis using Eqs. (10) and (11) such that

$$M_T = M(H \cos \theta, J_c^{ab}) \cos \theta + M(H \sin \theta, J_c^c) \sin \theta. \quad (13)$$

Figure 12 shows the calculated (solid line) as well as the experimental (solid circles) orientation dependence of the magnetization  $M_T$  for  $H=2000$  G,  $R=6.2$  mm,  $J_c^{ab}=8 \times 10^3$  A/cm<sup>2</sup>, and  $J_c^{ab}/J_c^c=5$ . The dotted line is  $M_T = -\mu_0 H \cos \theta$ . Interestingly, the parameters given above give rise to  $H/J_c^{ab}R < 1$  and  $H/J_c^cR > 1$ . Notice the different peak positions of the solid and dotted lines shown in Fig. 12. The peak position of these two curves can only coincide if  $J_c^{ab} \gg J_c^c$ . If  $J_c^c=0$ ,  $M_T = -\mu_0 H$  except when  $H \parallel ab$  plane for  $H/J_c^{ab}R \ll 1$ . For  $H/J_c^{ab}R > 1$ ,  $M_T$  behaves very much like a dipole. The small ‘‘satellite’’ peaks shown in the solid line of Fig. 12 are the result of the competition between these two limiting cases.

It should be noted that although the above calculation is performed for the superconducting sphere, the results we ob-

tained are not limited to the sphere geometry. The main factors that determine the features of the  $M$  vs  $H$  curve are the parameters  $H/J_cR$  and  $J_c^{ab}/J_c^c$ . It would be interesting to perform experiments for various values of  $H$ ,  $R$ , and  $J_c$  to probe the behavior of  $M_T(\theta)$  and to test the robustness of the assumptions made by the Bean model discussed here in layered superconductors.

#### ACKNOWLEDGMENTS

This work is supported by a grant from APRA/DSO (D.S., B.T., and D.Q.) and by the U.S. Department of Energy, Division of Materials Sciences, Office of Basic Energy Sciences under Contract No. DE-AC02-98CH10886 (Z.X.C.).

- 
- <sup>1</sup>D. Shi, D. Qu, S. Sagar, and K. Lahiri, *Appl. Phys. Lett.* **70**, 3606 (1997).
- <sup>2</sup>Brian Tent, D. Qu, and D. Shi (unpublished).
- <sup>3</sup>D. Shi, W. Zhong, U. Welp, S. Sengupta, V. Todt, G. W. Crabtree, S. Dorris, and U. Balachandran, *IEEE Trans. Magn. MAG-5*, 1627 (1994).
- <sup>4</sup>D. Shi, K. Lahiri, D. Qu, S. Sagar, V. F. Solovjov, and V. M. Pan, *J. Mater. Res.* **12**, 51 (1997).
- <sup>5</sup>D. Shi, K. Lahiri, J. R. Hull, D. LeBlanc, M. A. R. LeBlanc, A. Dabkowski, Y. Chang, Y. Jiang, Z. Zhang, and H. Fan, *Physica C* **246**, 253 (1995).
- <sup>6</sup>J. D. Jorgensen, *Jpn. J. Appl. Phys., Part 1* **26**, 2017 (1987).
- <sup>7</sup>W. K. Kwok, U. Welp, G. W. Crabtree, K. G. Vandervoort, R. Hulscher, and J. Z. Liu, *Phys. Rev. Lett.* **64**, 966 (1990).
- <sup>8</sup>E. M. Gyorgy, R. B. Dover, K. A. Jackson, L. F. Schneemeyer, and J. V. Waszczak, *Appl. Phys. Lett.* **55**, 238 (1989).
- <sup>9</sup>K. Kadowaki, J. N. Li, and J. J. Franse, *Physica C* **170**, 298 (1990).
- <sup>10</sup>U. Welp, W. K. Kwok, G. W. Crabtree, K. G. Vandervoort, and J. Z. Liu, *Phys. Rev. Lett.* **62**, 1908 (1989).
- <sup>11</sup>D. H. Kim, K. E. Gray, R. T. Kampwirth, J. C. Smith, D. S. Richeson, T. J. Marks, J. H. Kang, J. Talvacchio, and M. Eddy, *Physica C* **177**, 431 (1991).
- <sup>12</sup>K. E. Gray, *Appl. Supercond.* **2**, 295 (1994).
- <sup>13</sup>R. B. Goldfarb, in *Concise Encyclopedia of Magnetic & Superconducting Materials*, edited by J. Evetts (Pergamon, Oxford, 1992), p. 103.
- <sup>14</sup>W. Lo, D. A. Cardwell, C. D. Dewhurst, and S. L. Dung, *J. Mater. Res.* **11**, 786 (1996).
- <sup>15</sup>P. Diko, W. Gawalek, T. Habisreuther, T. Klupsch, and P. Goernert, *Phys. Rev. B* **52**, 13 658 (1995).
- <sup>16</sup>K. Salama, V. Selvamanickam, L. Gao, and K. Sun, *Appl. Phys. Lett.* **54**, 2352 (1989).
- <sup>17</sup>R. L. Meng, C. Kinalidis, and Y. Y. Sun, *Nature (London)* **345**, 326 (1990).
- <sup>18</sup>R. Weinstein, In-Gann Chen, J. Liu, D. Parks, V. Selvamanickam, and K. Salama, *Appl. Phys. Lett.* **56**, 1475 (1994).
- <sup>19</sup>Y. Nakamura, A. Endo, and Y. Shiohara, *J. Mater. Res.* **11**, 1094 (1996).
- <sup>20</sup>M. Cima, M. Flemings, A. Figueredo, M. Nakade, H. Ishii, H. Brody, and J. Haggerty, *J. Appl. Phys.* **72**, 179 (1992).